Brightest Cluster Galaxies: the centre can(not?) hold

Roberto De Propris[1], [*] Michael J. West[2], Felipe Andrade-Santos[3],
Cinthia Ragone-Figueroa[4,5], Elena Rasia[5,6], William Forman[3], Christine Jones[3],
Rain Kipper[7], Stefano Borgani[5,6,8,9] Diego García Lambas[4], Elena A. Romashkova[10]
and Kishore C. Patra[11]

[1]*FINCA, University of Turku, Vesilinnantie 5, Turku, 21400, Finland*
[2]*Lowell Observatory, 1400 W Mars Hill Rd, Flagstaff, AZ 86001, USA*
[3]*Harvard-Smithsonian Center for Astrophysics, 60 Garden Street, Cambridge, MA 02138, USA*
[4] *IATE, CONICET, Universidad Nacional de Córdoba, Laprida 854, X5000BGR, Córdoba, Argentina*
[5] *INAF, Osservatorio Astronomico di Trieste, via Tiepolo 11, I-34131, Trieste, Italy*
[6] *IFPU - Institute for Fundamental Physics of the Universe, Via Beirut 2, 34014 Trieste, Italy*
[7] *Tartu Observatory, University of Tartu, Observatooriumi 1, 61602 Tõravere, Estonia*
[8] *Dipartimento di Fisica dell' Universit'a di Trieste, Sezione di Astronomia, via Tiepolo 11, I-34131 Trieste, Italy*
[9]*INFN - National Institute for Nuclear Physics, Via Valerio 2, I-34127 Trieste, Italy*
[10]*Department of Physics, Massachusetts Institute of Technology, Cambridge, MA 02139, USA*
[11]*Department of Astronomy, University of California, Berkeley, CA 94720-3411, USA*

ABSTRACT

We explore the persistence of the alignment of brightest cluster galaxies (BCGs) with their local environment. We find that a significant fraction of BCGs do not coincide with the centroid of the X-ray gas distribution and/or show peculiar velocities (they are not at rest with respect to the cluster mean). Despite this, we find that BCGs are generally aligned with the cluster mass distribution even when they have significant offsets from the X-ray centre and significant peculiar velocities. The large offsets are not consistent with simple theoretical models. To account for these observations BCGs must undergo mergers preferentially along their major axis, the main infall direction. Such BCGs may be oscillating within the cluster potential after having been displaced by mergers or collisions, or the dark matter halo itself may not yet be relaxed.

Key words: galaxies: elliptical and lenticular, cD – galaxies: kinematics and dynamics

1 INTRODUCTION

In the hierarchical scenario with Λ Cold Dark Matter (CDM) cosmology, galaxies and clusters form by gradually accreting other halos over time, growing into progressively larger systems. The most massive halo eventually evolves to contain the brightest galaxy in the system, residing at the center of the cluster potential well and/or local density peaks (Beers & Geller 1983).

This Brightest Cluster Galaxy (hereafter BCG) is often a giant elliptical of the D or cD type (although not all BCGs are of this type). The BCG is often peculiar in terms of brightness, prevalence of AGN activity, colours, etc: (e.g., Tremaine & Richstone 1977; Lin et al. 2010; Hearin et al. 2013; Shen et al. 2014; Skibba et al. 2006, 2007; van den Bosch et al. 2007, 2008; Skibba & Sheth 2009; Vulcani et al. 2014).

One of the most unique properties of BCGs is the observed tendency for their major axes to share the same orientation as their host cluster (Sastry 1968; Binggeli 1982; Niederste-Ostholt et al. 2010;

Biernacka et al. 2015). This is believed to be a relic of their formation history, as it is found even at high redshifts both in observations (Li et al. 2013; West et al. 2017) and cosmological hydrodynamical simulations (Okabe et al. 2020b; Ragone-Figueroa et al. 2020). The conventional explanation is that the BCG lies at the centre of the forming cluster halo and accretes galaxies along a preferential direction (collimated infall) coinciding with the major accretion filament feeding the cluster growth within the cosmic web (e.g., West 1994; Dubinski 1998 see also Donahue et al. 2016; Okabe et al. 2020b,a; Ragone-Figueroa et al. 2020). This direction is then 'imprinted' on the shape of the growing BCG halo (and the tidal debris forming the intracluster light – Kluge et al. 2020) as well as that of the cluster in which it resides. Regarding cluster major mergers, it has been shown in a recent work (Ragone-Figueroa et al. 2020) that their frequency and geometry affect differently to the BCG alignment. Clusters that, after a major merger, are let to evolve without further major accretions are able to restore their alignments. Moreover, mergers along the cluster elongation axis can cause that, at the end of the accretion event, an even stronger alignment is developed.

These observations broadly support the 'central galaxy paradigm'

[*] E-mail: rodepr@utu.fi

defined by van den Bosch et al. (2005), in which the brightest galaxy lies at the centre of the dark matter halo. However, there is now evidence that this might not always be the case. Observations by van den Bosch et al. (2005); Skibba et al. (2011) and Lange et al. (2018) show that the brightest halo galaxy is displaced from the halo centre (as measured by the X-ray peak) in up to ∼ 40% of cases. In cluster environments, several authors find significant displacements between the position of the BCG and the dark matter halo (Sanderson et al. 2009; Zitrin et al. 2012; Hikage et al. 2013; Lauer et al. 2014; Martel et al. 2014; Oliva-Altamirano et al. 2014; Wang et al. 2014; Hoshino et al. 2015; Rossetti et al. 2016; Lopes et al. 2018; Zenteno et al. 2020), while Coziol et al. (2009) detect significant offsets from the cluster mean (peculiar velocities) in velocity space for about 1/3 of BCGs.

These off-centre BCGs are unexpected: the brightest (and most massive) cluster galaxy should occupy the centre of its halo and be at rest with respect to the X-ray gas and the velocity distribution of the cluster galaxies. Because of dynamical friction, a BCG should quickly fall to the cluster centre: indeed the observed fractions of off-centre BCGs are a factor of 2–3 higher than the predictions from the simulations of Croton et al. (2006); Monaco et al. (2007) and De Lucia & Blaizot (2007). The strength of these offsets is consistent with the bulk velocity seen in dark matter simulations (Behroozi et al. 2013): central galaxies may define the bottom of the potential well better than the dark matter halo (Beers & Geller 1983; Cui et al. 2016; Guo et al. 2016; Ye et al. 2017).

One possibility is that the BCG is actually not at rest with respect to the cluster centre (e.g., it may have been displaced by mergers or recently infallen), another is that the dark matter halo may not be in equilibrium. There are known cases where the BCG does not appear to be at rest with respect to the frame defined by the other galaxies (Barbosa et al. 2018) and examples where the X-ray gas appears to be sloshing (Markevitch et al. 2001; Churazov et al. 2003; Johnson et al. 2012; Harvey et al. 2017). However, we expect that dynamical friction should quickly damp any oscillation of the BCG in a relaxed dark matter halo, whereas a non-relaxed halo should produce peculiar velocities of the order of 20–30% of the velocity dispersion of the dark matter halo (Yoshikawa et al. 2003; Ye et al. 2017), that is broadly in agreement with the observed spatial and dynamical offsets for BCGs.

If this is the case, however, then why are BCGs still aligned with the cluster galaxy distribution? One may naively expect that if BCGs are moving within the cluster potential they would not necessarily maintain their original alignment (they could of course be displaced mainly along the accretion axis). If BCGs are not truly in the centre, then the origin of the alignment effect and its long-term preservation via collimated infall may be difficult to explain.

In this paper we re-examine the question of BCG offsets and we produce a comprehensive study of the displacement between BCGs and the centre of clusters' X-ray halos. We examine whether such displaced BCGs also show peculiar velocities with respect to the cluster mean. Finally we measure the alignment effect for BCGs at rest and offset BCGs. In the following section we describe our selection of clusters, identification of the BCG, measurement of its position axis, measurement of the position axis of the X-ray halo and of the peculiar velocities. In section 3 we show our results: we assess the frequency for BCGs to be significantly displaced from the centre of the X-ray halo and to have significant peculiar velocity with respect to the cluster mean; we measure the alignment effect and whether it depends on the offset from the cluster centre or mean velocity. Finally, we discuss the implications of our results in section 4. We assume the latest cosmological parameters from the Planck
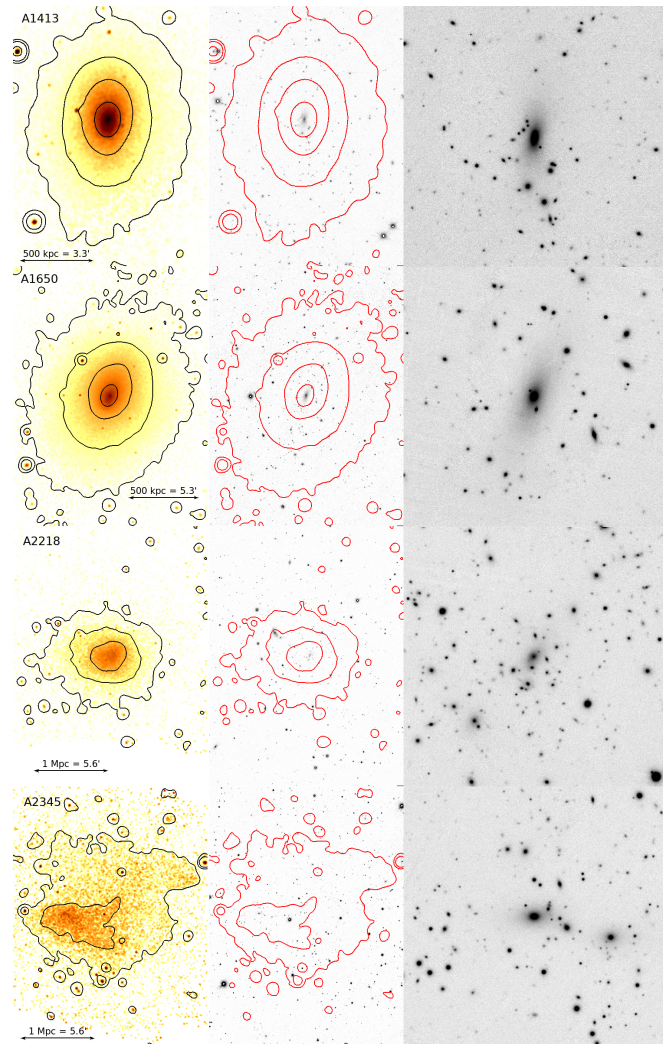
Figure 1. X-ray and optical images of several clusters from the *Chandra-Planck Legacy Program for Massive Clusters of Galaxies*. The left panels show $0.5 - 2.0$ keV, background-subtracted, exposure-map-corrected ACIS-I images from *Chandra*. The middle panels show the X-ray contours overlaid on r-band images of the same fields from the Pan-STARRS survey. The rightmost panels zoom into a $200'' \times 200''$ region centered on each BCG.

Collaboration for the remainder of this paper (Planck Collaboration et al. 2018).

2 DATA

We identified two independent cluster samples, one X-ray-selected and the other velocity-selected, as described below.

2.1 X-ray-selected cluster sample

Our first cluster sample is taken from Andrade-Santos et al. (2017), which consists of 164 clusters in the Planck Early Sunyaev-Zel'dovich sample with $z \leqslant 0.35$ plus a flux-limited X-ray sample of 100 clusters with $z \leqslant 0.30$, with some overlap. All have *Chandra* observations obtained as part of the *Chandra-Planck Legacy Program for Massive*

Clusters of Galaxies[1], with exposures that yield at least 10,000 source counts. Optical imaging is provided by data from the Panoramic Survey Telescope and Rapid Response System (Pan-STARRS) survey Chambers et al. (2016); Magnier et al. (2016) to identify and measure the properties of BCGs. We choose the BCG as the brightest galaxy from the Pan-STARRS stacked image (as in Fig. 1) over a 3 Mpc region centred on the X-ray peak. In general, BCGs have distinctive appearances, dominant ellipticals often surrounded by extended halos of diffuse starlight, so identification is usually unambiguous. In cases of merging clusters or subclusters, we opted to use only the primary component in order to focus on the most massive systems. All these clusters also have redshift information, with some overlapping with our second sample (see below).

Chandra images were processed following standard procedures described in Vikhlinin et al. (2005) and using calibration files CALDB 4.7.2 and 4×4 binning. Each image was further processed using the *csmooth* routine in the CIAO software package (Fruscione et al. 2006), which uses the adaptive smoothing algorithm of Ebeling et al. (2006) to create a smoothed map of the X-ray emission. Sliding cell convolution with a Gaussian smoothing kernel was found to be optimal for robust determination of cluster position angles. A few examples are shown in Fig. 1. The resolution of the *Chandra* corresponds to ~ 1 to 10 kpc depending on the cluster redshifts, with a median resolution element of 3.5 kpc.

The projected orientation of each cluster's principal axis on the plane of the sky was determined using Source Extractor (Bertin & Arnouts 1996), which computes luminosity-weighted moments of the smoothed X-ray flux using all pixels above a 3-σ threshold relative to the background. The cluster positions angles are listed in Table 1. This shows the cluster, any other common name, the redshift, position angle of the cluster major axis, position angle of the BCG major axis and selection (X for X-rays and V for velocities, see below). We show the first few lines and make the remainder of the table available electronically. A direct comparison with position angles derived from poorer-resolution *Einstein* observations (West et al. 1995) shows good agreement, with a median absolute difference of $\pm 13°$.

2.2 Velocity-selected cluster sample

Because BCGs can be offset from the cluster centre in position and/or velocity space, we compiled a second cluster sample by selecting all clusters with 50 or more member galaxies based on available velocities in NED. The sample is heterogeneous but contains mainly Abell clusters plus some systems from the HeCS survey (Rines et al. 2016, 2018) not present in the Abell catalog. This sample selection does not depend on X-ray emission, providing an independent check of BCG alignments when the galaxy is not at rest relative to the gravitational potential (e.g., see Martel et al. 2014). As we require 50 or more spectroscopic redshifts per cluster, these are likely to be comparatively massive systems.

For all clusters we used images from PanStarrs1 to identify the brightest cluster galaxy (within approximately the Abell radius) and take this as the cluster center. We then retrieved all available redshifts within the r_{200} radius (Carlberg et al. 1997) of each cluster. We then used a 'double gapping' method (as in Zabludoff et al. 1990; De Propris et al. 2002) to identify the velocity peak corresponding to the cluster. We sort all galaxies by velocity and require that the initial sample of cluster galaxies is separated by 1000 km s^{-1} gaps from

the next galaxy in velocity space (i.e., the closest likely non cluster member). We then compute the cluster mean velocity (location) and velocity dispersion (scale) using robust methods, as described by Beers et al. (1990), using the *R* code library (R Core Team 2013). We then repeat our selection by requiring that the above 'gaps' are 3 times this measured velocity dispersion and obtain the final mean velocity and velocity dispersion using the same procedure. We require that a minimum 50 velocities are left after the first selection. These velocity dispersions are also given in Table 1.

Cluster position angles are derived from the projected distribution of member galaxies on the plane of the sky as described in West et al. (2017). This is done by computing the moments of inertia of the galaxy distribution. Information for this sample can be found in Table 1 as well. For clusters in common with the X-ray selected sample the median difference in the position angle of the BCG is $15.8°$.

2.3 BCG sample

For all clusters, the BCG was identified and its properties determined using data from the Pan-STARRS PS1 survey. SDSS *r*-band images of each cluster field were downloaded as *fits* files from the PanSTARRS-1 database hosted at the Space Telescope Science Institute. Because the PS1 declination limit is $\delta \geq -30$ deg, BCGs and their host clusters at more southerly declinations were removed from the sample. In most cases the BCG was easily identifiable from visual inspection of the PS1 images. In a few instances, however, multiple BCG candidates of comparable brightness could be seen, and so the brightest galaxy near the X-ray centroid was chosen. The sample was culled of any candidate BCG fainter than $M_r = 22$ to ensure that our study focuses on the most massive galaxies. A detailed comparison of our selected BCGs with those identified in other papers (Stott et al. 2008; Coziol et al. 2009; Lauer et al. 2014; Rossetti et al. 2016; Lopes et al. 2018) shows excellent agreement in general. In those few cases where there was disagreement it likely comes down to different choices among several plausible BCG candidates.

Having identified the BCGs, their positions and apparent *r*-band (Kron) magnitudes were obtained from the Pan-STARRS DR2 catalog. Each galaxy's projected distance from the X-ray centroid of its host cluster given by Andrade-Santos et al. (2017) and its absolute magnitude, M_r, were calculated using the most recent cluster redshifts in the NASA Extragalactic Database. As expected, the BCGs have typical absolute magnitudes $M_r \simeq -22$ to -23 mag and, with few exceptions, generally reside at or near the cluster center, most within a few tens of kpc. Source Extractor was used to measure the projected orientation of each BCG's major axis and these values are listed in Table 1.

Fig. 1 shows several examples of BCGs and their host clusters. Our final samples consist of 124 X-ray-selected clusters and 136 velocity-selected clusters, with 52 clusters common to both. Many of these clusters are well-known Abell clusters.

2.4 Cosmological Hydrodynamical Simulations

The set of cosmological hydrodynamocal simulations that we analyse in this work has already been presented in Ragone-Figueroa et al. (2018) where it has proven to reproduce realistic BCG mass evolution histories. Furthermore, we have used it recently to assess the BCG-Cluster alignment evolution in the last 10 Gyr (Ragone-Figueroa et al. 2020). The simulations are similar to those presented in Ragone-Figueroa et al. (2013), but with an updated version of the AGN feedback scheme.

---

[1] https://hea-www.harvard.edu/CHANDRA_PLANCK_CLUSTERS

Table 1. Clusters and properties of BCGs (sample of full online version)

Name	Other name	z	Cluster PA	BCG PA	σ (km s^{-1})	Selection
EXO0422		0.038	-17.8	-9.9		X
Hydra A		0.055	-36.8	-23.3		X
IC 1262		0.033	49.7	77.2		X
RXJ1958.2-3011		0.117	-17.8	35.4		X
A7		0.106	-44.9	-49.2	1072	V
A21		0.095	-26.0	-27.5	910	V
A85	G115.16-72.09	0.055	-29.5/-17.6	-29.6	970	XV
XMMUJ0044.0-2033	G106.73-83.22	0.292	30.5	-9.0		X
AS0084		0.108	-77.5	-73.2	717	V
A115	G124.21-36.48	0.197	-42.6	-32.0	1730	X
A119	G125.58-64.14	0.044	37.9/35.9	34.2	843	XV
A133	G149.55-84.16	0.057	24.6/32.1	23.2	700	XV

The set consists of 29 zoomed-in Lagrangian regions evolved with a custom version of the GADGET-3 code (Springel 2005) and originally selected from a gravity-only simulation of 1 h^{-1}Gpc box. Part of the re-simulated regions are centered in the 24 most massive dark matter (DM) haloes of the parent cosmological volume and have masses $M_{200} \gtrsim 1.1 \times 10^{15}$ M$_\odot$[2]. In addition, we randomly select 5 less massive haloes with masses $1.4 \times 10^{14} \lesssim M_{200} \lesssim 6.8 \times 10^{14}$ M$_\odot$. Each region was re-simulated at higher resolution including hydrodynamics and all the sub-resolution baryonic physics usually taken into account in galaxy formation simulations (cooling, star formation and associated feedback, metal enrichment, AGN feedback).

The adopted cosmological parameters are: $\Omega_m = 0.24$, $\Omega_b = 0.04$, $n_s = 0.96$, $\sigma_8 = 0.8$ and $H_0 = 72$ km s^{-1} Mpc^{-1}. The mass resolution for the DM and gas particles is $m_{DM} = 8.47 \times 10^8$ h^{-1} M$_\odot$ and $m_{gas} = 1.53 \times 10^8$ h^{-1} M$_\odot$, respectively. For the gravitational force, a Plummer-equivalent softening length of $\epsilon = 5.6$ h^{-1} kpc is used for DM and gas particles, whereas $\epsilon = 3$ h^{-1} kpc for black hole and star particles. The DM softening length is kept fixed in comoving units for $z > 2$ and in physical units at lower redshift. For further details on this set of simulations, we refer the reader to the above mentioned papers.

The re-simulated volumes are chosen to be large enough so that by z=0 no DM particles from the low-resolution region are found within 5 virial radii from the center of the target cluster. For this reason, more clusters might be present in the same Lagrangian region. In particular for this work, we selected, among the two most massive clusters in each box, those which at z=0 have at least 50 galaxies (with stellar masses > 1×10^{10} M$_\odot$). This selection criterion leads us to a sample of 38 clusters. The M_{200} distribution at redshift zero has a median of 1.47×10^{15} M$_\odot$ and 25% and 75% percentiles of 6.80×10^{14} M$_\odot$ and 1.75×10^{15} M$_\odot$, respectively.

As for the BCGs, they are defined as the stellar particles inside 0.1 r_{500} radius. This radius is similar to that at which our simulated BCGs reach a rest-frame surface brightness of $\mu_V \sim 24$ mag arcsec^{-2} (Ragone-Figueroa et al. 2018), a classical observational value to define the galaxy limit (de Vaucouleurs et al. 1991). At reshift zero, the BCGs mass distribution median is 2.16×10^{12} M$_\odot$ and the 25% and 75% percentiles are 1.3 and 2.74 $\times 10^{12}$ M$_\odot$, respectively.

---

[2] M_{200} is the mass enclosed by a sphere whose mean density is 200 times the critical density at the considered redshift. The radius of this sphere is dubbed R_{200}
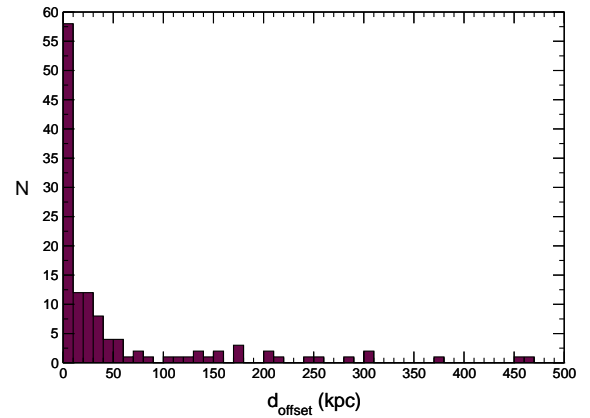
Figure 2. The distribution of projected distances between BCGs and the peak of the X-ray emission in their host clusters. Most BCGs reside at or very near the X-ray centroid. However a few are found tens or even hundreds of kpc away.

3 RESULTS

3.1 BCG offsets

Fig. 2 shows the distribution of projected offsets between the position of the BCG and the X-ray peak. The great majority of BCGs in our sample lie within a few tens of kpc of the X-ray centroid – the median separation for the X-ray-selected sample is ~ 15 kpc, consistent with other previous studies (Lauer et al. 2014; Rossetti et al. 2016; Lopes et al. 2018) and comparable in size to the effective radii of the galaxies themselves (Stott et al. 2011). For comparison, Zitrin et al. (2012) finds distribution of displacements between the BCG and the centre of the DM halo peaked on zero, with a rms displacement of 13 kpc, a result consistent with our estimate above.

Similarly, Fig. 3 shows the distribution of BCG velocity offsets from the cluster mean for this sample. Martel et al. (2014) argue that these are a more accurate measure of true offsets than shifts from the cluster centroid in projected position on the sky. The BCG peculiar velocities have been normalized by the cluster velocity dispersion (scale). The median velocity offset for the sample is $V_{BCG}/\sigma = 0$, with a median *absolute* BCG peculiar velocity $V_{BCG}/\sigma \sim 0.26$,
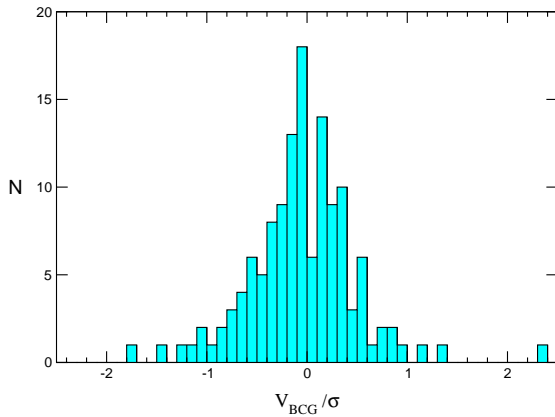
Figure 3. The distribution of BCGs peculiar velocities, defined as the difference between the BCG's radial velocity and the cluster location (the robust statistical equivalent of the cluster mean velocity) normalized by the cluster scale (the robust equivalent of the cluster velocity dispersion).
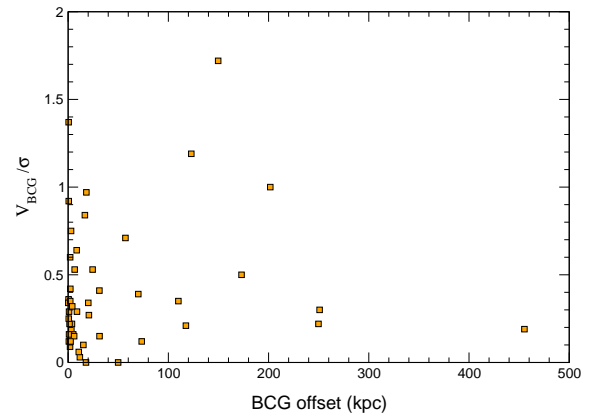
Figure 4. The distribution of BCGs peculiar velocities versus projected distance from the X-ray centroid for 52 clusters. No obvious correlation is seen.

corresponding to typical peculiar velocities of $\sim$ 100 to 200 km/s. Typical velocity errors are those of the surveys (mainly SDSS and 2dF) these velocities are largely drawn from, i.e., a few 10s of $\mathrm{km\,s^{-1}}$. These results indicate that a significant fraction of these BCGs are in motion within the cluster potential. Our estimate compares well with Coziol et al. (2009) where BCGs had a median $\Delta V/\sigma$ of 0.32, despite their fewer velocities and less robust statistics and the estimate for poorer clusters in the COSMOS field by Gozaliasl et al. (2020): the slightly lower value we report comes from our selection of clusters with larger velocity samples and our use of the median absolute deviation methods. The displacements are statistically significant: we carried out a Monte Carlo simulation with 50 galaxies sampled from a random Gaussian distribution and recovered the same mean velocity within 0.6% with a dispersion of 15%.

Fig. 4 compares the velocity offsets with offsets from the X-ray centroid for the 52 BCGs common to both samples. No correlation is seen. This is quite surprising as, if the BCGs are displaced by mergers, one expects that shifts from the centre of the potential well also result in peculiar velocities. One possibility is that some or most of the momentum is absorbed by the intracluster medium. However, while most BCGs have small peculiar velocities, it is clear that a non-neglible faction are not at rest with respect to the cluster dynamical center.

3.2 BCG alignments

We first examine the general tendency for BCGs to share the same orientation as their host cluster in the X-ray selected sample. As Fig. 5 shows, a strong alignment tendency is evident. To assess the statistical significance of these alignments, we use three different tests for isotropy: the Kuiper V, Rao spacing, and binomial tests (see West et al. (2017) for a description of these statistical tests). The probability that the BCGs have random orientations with respect to their host clusters is minuscule ($\ll$ 1%) according to these metrics.

Fig. 6 shows these same alignments as a function of BCG distance from the cluster X-ray centroid. Remarkably, the BCGs are aligned even when they do not reside at the cluster centre, for separations up to as much as $\sim$ 200 kpc. For larger offsets, Fig. 6 hints that the BCGs
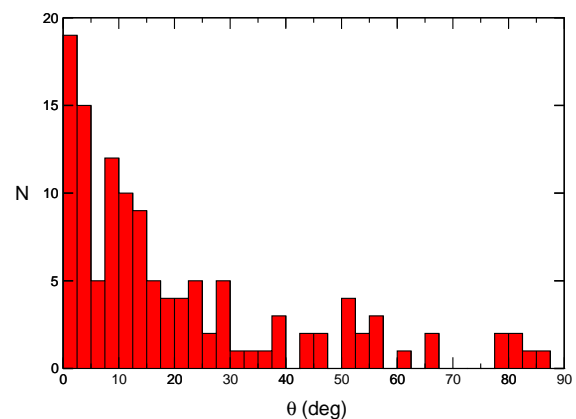
Figure 5. BCG alignments for the X-ray-selected clusters. Here θ is the acute angle between the projected major axis of each galaxy and that of the cluster in which it resides. If the galaxy and cluster axes are perfectly aligned then $\theta = 0°$, while random galaxy orientations will produce a uniform distribution between 0° and 90°. The BCGs exhibit a strong tendency to align with their host clusters. This is confirmed by the Kuiper V, Rao and binomial statistical tests, which all indicate a probability $p \ll 1\%$ that the observed distribution of angles is consistent with random BCG orientations.

might be more randomly orientated, however no firm conclusion is possible because of the small numbers of galaxies.

In Fig. 7, we examine the direction of BCG offsets by comparing the vector defined by the galaxy's projected position relative to the X-ray centroid with the orientation of the host cluster's major axis. There is a clear anisotropy in these offsets, with the BCGs preferentially displaced along the direction of the cluster major axis rather than in random directions. The Kuiper and binomial tests both confirm that the distribution seen in Fig. 7 has a probability much less than 1% of being consistent with random directional offsets, while the Rao test indicates a probability $p \sim 2\%$.

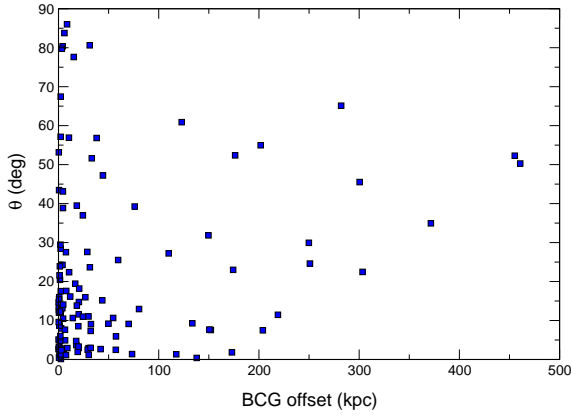We next examine the relation between BCG peculiar velocity and

Figure 6. BCG alignments as a function of the galaxy's projected distance from the X-ray centroid of its host cluster.
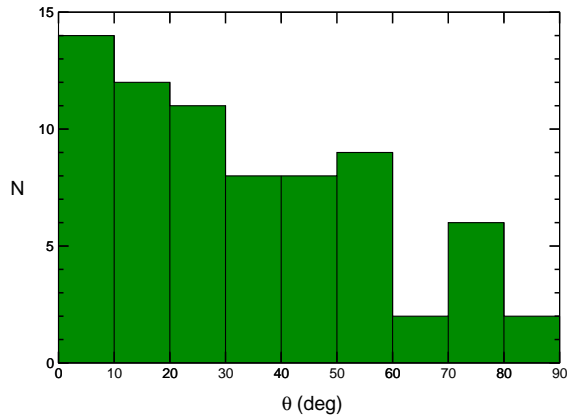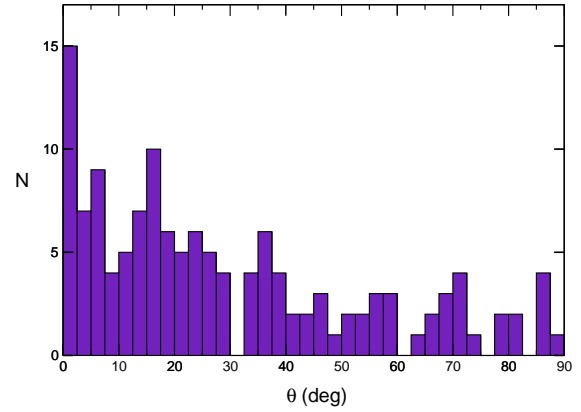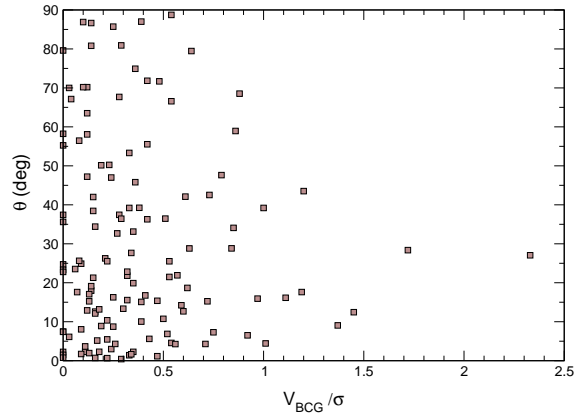

Figure 8. BCG alignments for the sample of velocity-selected clusters. As in Fig. 5, θ is the acute angle between the projected major axis of each galaxy and that of the cluster in which it resides. Cluster position angles were determined from moments of inertia of the projected galaxy distribution. The Kuiper V, Rao, and binomial statistical tests all indicate a probability $p \ll 1\%$ that the observed distribution of angles is consistent with random BCG orientations.

Figure 7. The direction of BCG offsets from the X-ray centroid compared to the overall cluster orientation. Here θ is the acute angle between the direction of BCG offset and the orientation of the cluster major axis. Only those clusters whose BCG is offset by more than twice the *Chandra* resolution are included here, a total of 72 clusters. These results reveal a tendency for the BCG to be offset preferentially along the cluster major axis. This is confirmed by the Kuiper V, Rao, and binomial statistical tests, which all indicate a probability $p < 1\%$ that the observed distribution of offset directions is consistent with random.

Figure 9. BCG alignments as a function of peculiar velocity. Here $\Delta V_{BCG}/\sigma$ is the absolute difference between the BCG's velocity and the mean cluster velocity, and σ is the cluster velocity dispersion.

alignment tendency. Fig. 8 shows the alignment of BCGs in the velocity-selected clusters. Again a strong general tendency for these galaxies to align with their host clusters is evident. Fig. 9 plots the alignments as a function of BCG peculiar velocity; it appears that BCG alignments with their host clusters are largely independent of whether or not the galaxy is at rest with respect to the cluster.

4 DISCUSSION

The main findings of this paper are:

(i) A significant fraction of BCGs have spatial offsets of a few tens of kpc or more from the centroid of the X-ray light distribution that presumably traces the centre of the dark matter halo and reflects the cluster's dynamical state. Compared with theoretical models, these offsets are much larger than the expected 'wobble' around the centre of a standard Cold Dark Matter halo (< 2 kpc vs. a few tens of kpc) as in the simulations of Kim et al. (2017) and Harvey et al. (2017). However, the X-ray gas may not trace the dark matter halo distribution (e.g., by gas sloshing, etc.)

(ii) A significant number of BCGs also have significant line-of-sight peculiar velocities relative to the cluster. These observations suggest that many BCGs are not currently at rest in the potential well of their host cluster.

(iii) Despite the prevalence of BCG displacements, these galaxies still show a strong tendency to share the same orientation as the cluster in which they reside (cf. Tempel et al. 2013, a remarkably robust coherence of structures over scales from tens to thousands of kpc, as suggested by the simulations of Rhee et al. (2017)

4.1 Comparison of Observations with Simulations

The computation of the cluster and BCG elongation axes is done as in Ragone-Figueroa et al. (2020). They are obtained from the principal axes of the ellipsoids that best describe the corresponding distribution of matter. For the purposes of this work cluster principal axes and center of mass are obtained using dark matter particles within r_{200}. While for obtaining BCG principal axes we use star particles inside $0.1\, r_{500}$.

Fig. 10 shows the distributions of BCG offsets in position and velocity as well as their correlations with the BCG-Cluster alignment angle, in full 3D space (4 left-hand panels) and in projection and radial velocity (4 right-hand panels). We find in simulations galaxies with significant offsets, in projected space the mean(median) offset is ~ 53kpc(78kpc), which is larger that the mean found in the observational data (~ 15kpc). Conversely, the mean(median) normalized 1D BCG velocity $|V_{BCG}/\sigma|$ (with respect to the cluster mean) is $\sim 0.09(0.07)$, which is lesser than in the data (0.26). The maximum $\Delta V/\sigma$ in these simulations is lower than that observed because of the smaller number of simulated cluster samples.

BCGs in these simulations also have a tendency to be aligned with the cluster major axis. Indeed, in Ragone-Figueroa et al. (2020) it was shown that the signal of alignment is present since $z \lesssim 1.5$. There is broad agreement between these simulations and the observational data on this regard. Namely, the alignment is still significant (within $\pm 20°$) for off-centre BCGs and shows no dependence on the BCG velocity with respect to the cluster mean. As shown in Fig. 4 for the observations, Fig. 11 reveals no evident correlation between BCGs offsets and velocities.

In order to further analyse the persistence of the alignment, we reconstruct the evolutionary path of each one of the 38 clusters. We follow back in time the cluster main progenitor from $z = 0$ to $z = 2$ using 60 simulation outputs. We find that in the studied redshift range simulated BCG offset directions are not randomly oriented. Fig. 12 shows the median of the angle between the BCG offset and the cluster DM elongation axis as a function of time. This fact together with the persistence of the alignment in off-centre BCGs, suggest that BCGs lay preferentially along the cluster major axis. The cluster's major axis defines the direction of least resistance of BGC motion and the direction along which mergers preferentially occur. Mergers (if they are the cause of the BCG offsets) may therefore take place along a preferential accretion direction, as in the collimated infall models of West (1994) and Dubinski (1998).

5 CONCLUSIONS

The observations suggest that even in very high mass halos the central galaxy paradigm does not hold in a large fraction of cases, much larger than one would expect from the predictions of numerical codes (van den Bosch et al. 2005). In some cases, this may be due to the mis-identification of a satellite as the central galaxy as the former is not necessarily less bright or less massive than the latter. However, galaxies with position and/or velocity offsets cannot all be explained in this fashion. There are two possibilities: the BCG is still moving within the cluster potential towards the bottom of the potential well or the halo is unrelaxed and oscillates.

The persistence of the alignment effect even for offset galaxies would tend to support the latter scenario where the halo is not relaxed and the BCG is at rest with respect to all other galaxies. This is borne out by observations for most galaxies. However, the persistence of alignments even for galaxies with a velocity offset, at least until the peculiar velocity is $< 40\%$ of the velocity dispersion, is unexpected, as in this case the BCG is not moving with the rest of the galaxies as in the non-relaxed halo picture. One possibility is that these are cases where the BCG is displaced by a recent collision or cluster merger, and that these collisions occur preferentially along the dominant accreting filament.

Another possibility is that the BCG is actually moving around a constant density core rather than a CDM cusp (Kim et al. 2017; Harvey et al. 2017): the significant peculiar velocities would tend to support this. The BCG may slosh around such a core for long periods after a cluster merger, although the persistence of the alignment effect may be more difficult to maintain in this case.
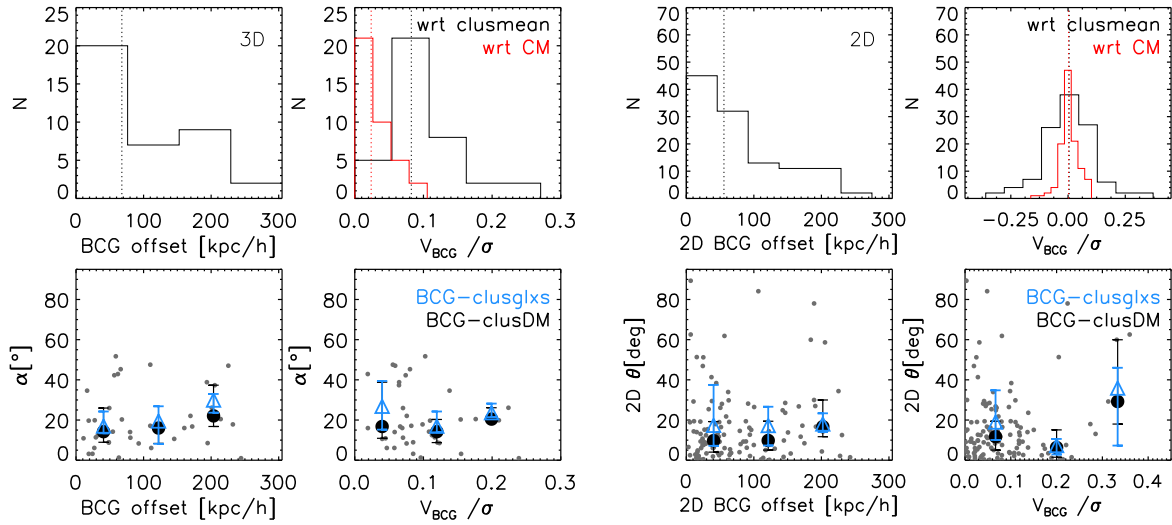
Figure 10. The four left-hand panels correspond to full 3D position and velocity space: Top panels show the distributions and medians of BCG offsets from the DM CM of clusters (left) and BCG velocities (BCG velocity with respect to the cluster-mean-velocity/DM-CM in black/red) normalized to its cluster velocity dispersion (right), respectively. Bottom panels show the 3D BCG alignment with the cluster galaxies (blue) and DM (black) as a function of the BCG offset (left) and the velocity with respect to the cluster mean (right). The four panels on the right-hand side show the same quantities but in projected space and 1D radial velocities. Here, the 114 dots are obtained from the original 38 clusters performing projections along the 3 Cartesian axes. The median of the |1D V_{BCG}/σ| distribution is ~0.07 and 0.02 depending on whether the BCG velocity is computed with respect to the cluster mean or the cluster DM CM, respectively. Large dots and bars in all panels correspond to medians and 25%-75% percentiles, respectively, per bin of the corresponding offset.
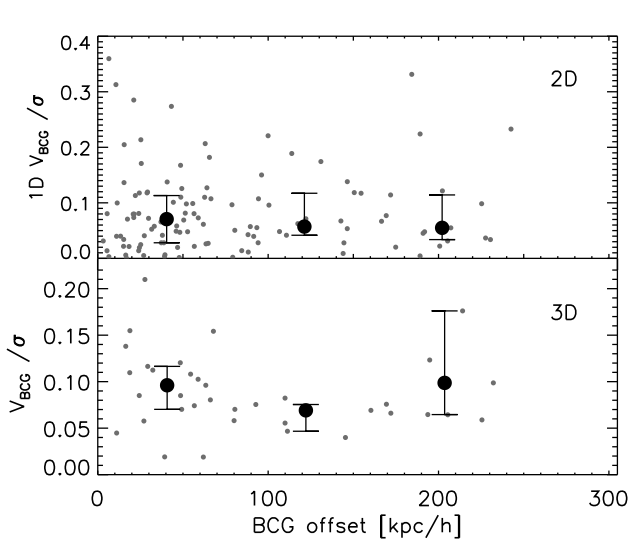

Figure 11. Top panel shows the dependence of the |1D V_{BCG}/σ| on the projected BCG offset. The same in bottom panel but for the full 3D quantities. BCG velocities are computed with respect to the cluster mean.
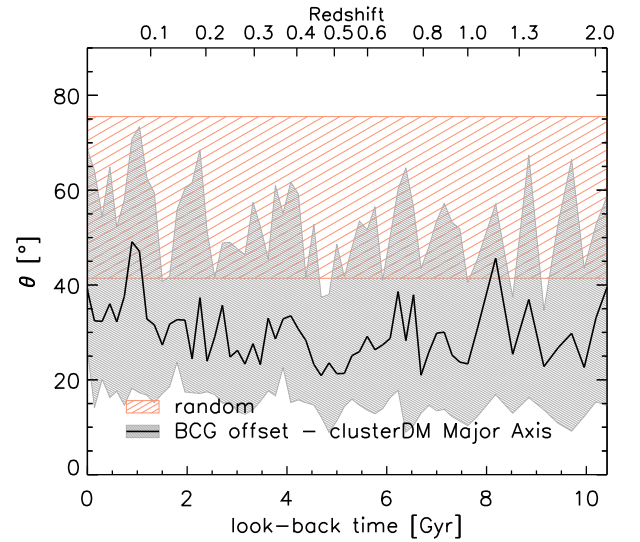

Figure 12. The direction of the BCG offsets from the clusterCM is not randomly oriented with respect to the cluster elongation in the last ~ 10 Gyr. Black solid line shows, as a function of look-back time, the median 3D angle between the direction of the BCG offset from the cluster DM center of mass and the direction of the cluster DM major axis. If these two directions were randomly oriented then it is expected a median $\theta = 60°$ and 25% 75% percentiles of ~ 41.4° and ~ 75.5°, respectively

Note added: We want to point out that comparable BCG velocity offsets were previously identified by Lauer et al (2014), who also found a correlation between BCG morphology and displacement.

DATA AVAILABILITY

The data underlying this article are available in the article and in its online supplementary material.

REFERENCES

Andrade-Santos F., et al., 2017, ApJ, 843, 76

Barbosa C. E., Arnaboldi M., Coccato L., Gerhard O., Mendes de Oliveira C., Hilker M., Richtler T., 2018, A&A, 609, A78

Beers T. C., Geller M. J., 1983, ApJ, 274, 491

Beers T. C., Flynn K., Gebhardt K., 1990, AJ, 100, 32

Behroozi P. S., Wechsler R. H., Wu H.-Y., 2013, ApJ, 762, 109

Bertin E., Arnouts S., 1996, A&AS, 117, 393

Bertocco S., et al., 2019, arXiv e-prints, p. arXiv:1912.05340

Biernacka M., Panko E., Bajan K., Godłowski W., Flin P., 2015, ApJ, 813, 20

Binggeli B., 1982, A&A, 107, 338

Carlberg R. G., et al., 1997, ApJ, 485, L13

Chambers K. C., et al., 2016, arXiv e-prints, p. arXiv:1612.05560

Churazov E., Forman W., Jones C., Böhringer H., 2003, ApJ, 590, 225

Coziol R., Andernach H., Caretta C. A., Alamo-Martínez K. A., Tago E., 2009, AJ, 137, 4795

Croton D. J., et al., 2006, MNRAS, 365, 11

Cui W., et al., 2016, MNRAS, 456, 2566

De Lucia G., Blaizot J., 2007, MNRAS, 375, 2

De Propris R., et al., 2002, MNRAS, 329, 87

Donahue M., et al., 2016, ApJ, 819, 36

Dubinski J., 1998, ApJ, 502, 141

Ebeling H., White D. A., Rangarajan F. V. N., 2006, MNRAS, 368, 65

Fruscione A., et al., 2006, in Proc. SPIE. p. 62701V, doi:10.1117/12.671760

Gozaliasl G., et al., 2020, A&A, 635, A36

Guo H., et al., 2016, MNRAS, 459, 3040

Harvey D., Courbin F., Kneib J. P., McCarthy I. G., 2017, MNRAS, 472, 1972

Hearin A. P., Zentner A. R., Newman J. A., Berlind A. A., 2013, MNRAS, 430, 1238

Hikage C., Mandelbaum R., Takada M., Spergel D. N., 2013, MNRAS, 435, 2345

Hoshino H., et al., 2015, MNRAS, 452, 998

Johnson R. E., Zuhone J., Jones C., Forman W. R., Markevitch M., 2012, ApJ, 751, 95

Kim S. Y., Peter A. H. G., Wittman D., 2017, MNRAS, 469, 1414

Kluge M., et al., 2020, ApJS, 247, 43

Lange J. U., van den Bosch F. C., Hearin A., Campbell D., Zentner A. R., Villarreal A., Mao Y.-Y., 2018, MNRAS, 473, 2830

Lauer T. R., Postman M., Strauss M. A., Graves G. J., Chisari N. E., 2014, ApJ, 797, 82

Li C., Jing Y. P., Faltenbacher A., Wang J., 2013, ApJ, 770, L12

Lin Y.-T., Ostriker J. P., Miller C. J., 2010, ApJ, 715, 1486

Lopes P. A. A., Trevisan M., Laganá T. F., Durret F., Ribeiro A. L. B., Rembold S. B., 2018, MNRAS, 478, 5473

Magnier E. A., et al., 2016, arXiv e-prints, p. arXiv:1612.05240

Markevitch M., Vikhlinin A., Mazzotta P., 2001, ApJ, 562, L153

Martel H., Robichaud F., Barai P., 2014, ApJ, 786, 79

Monaco P., Fontanot F., Taffoni G., 2007, MNRAS, 375, 1189

Niederste-Ostholt M., Strauss M. A., Dong F., Koester B. P., McKay T. A., 2010, MNRAS, 405, 2023

Okabe T., et al., 2020a, arXiv e-prints, p. arXiv:2005.11469

Okabe T., et al., 2020b, MNRAS, 491, 2268

Oliva-Altamirano P., et al., 2014, MNRAS, 440, 762

Planck Collaboration et al., 2018, arXiv e-prints, p. arXiv:1807.06209

R Core Team 2013, R: A Language and Environment for Statistical Computing. R Foundation for Statistical Computing, Vienna, Austria, http://www.R-project.org/

Ragone-Figueroa C., Granato G. L., Murante G., Borgani S., Cui W., 2013, MNRAS, 436, 1750

Ragone-Figueroa C., Granato G. L., Ferraro M. E., Murante G., Biffi V., Borgani S., Planelles S., Rasia E., 2018, MNRAS, 479, 1125

Ragone-Figueroa C., Granato G. L., Borgani S., De Propris R., García Lambas D., Murante G., Rasia E., West M., 2020, MNRAS, 495, 2436

Rhee J., Smith R., Choi H., Yi S. K., Jaffé Y., Candlish G., Sánchez-Jánssen R., 2017, ApJ, 843, 128

Rines K. J., Geller M. J., Diaferio A., Hwang H. S., 2016, ApJ, 819, 63

Rines K. J., Geller M. J., Diaferio A., Hwang H. S., Sohn J., 2018, ApJ, 862, 172

Rossetti M., et al., 2016, MNRAS, 457, 4515

Sanderson A. J. R., Edge A. C., Smith G. P., 2009, MNRAS, 398, 1698

Sastry G. N., 1968, PASP, 80, 252

Shen S., Yang X., Mo H., van den Bosch F., More S., 2014, ApJ, 782, 23

Skibba R. A., Sheth R. K., 2009, MNRAS, 392, 1080

Skibba R., Sheth R. K., Connolly A. J., Scranton R., 2006, MNRAS, 369, 68

Skibba R. A., Sheth R. K., Martino M. C., 2007, MNRAS, 382, 1940

Skibba R. A., van den Bosch F. C., Yang X., More S., Mo H., Fontanot F., 2011, MNRAS, 410, 417

Springel V., 2005, MNRAS, 364, 1105

Stott J. P., Edge A. C., Smith G. P., Swinbank A. M., Ebeling H., 2008, MNRAS, 384, 1502

Stott J. P., Collins C. A., Burke C., Hamilton-Morris V., Smith G. P., 2011, MNRAS, 414, 445

Taffoni G., Becciani U., Garilli B., Maggio G., Pasian F., Umana G., Smareglia R., Vitello F., 2020, arXiv e-prints, p. arXiv:2002.01283

Tempel E., Stoica R. S., Saar E., 2013, MNRAS, 428, 1827

Tremaine S. D., Richstone D. O., 1977, ApJ, 212, 311

Vikhlinin A., Markevitch M., Murray S. S., Jones C., Forman W., Van Speybroeck L., 2005, ApJ, 628, 655

Vulcani B., et al., 2014, ApJ, 797, 62

Wang L., et al., 2014, MNRAS, 439, 611

West M. J., 1994, MNRAS, 268, 79

West M. J., Jones C., Forman W., 1995, ApJ, 451, L5

West M. J., de Propris R., Bremer M. N., Phillipps S., 2017, Nature Astronomy, 1, 0157

Ye J.-N., Guo H., Zheng Z., Zehavi I., 2017, ApJ, 841, 45

Yoshikawa K., Jing Y. P., Börner G., 2003, ApJ, 590, 654

Zabludoff A. I., Huchra J. P., Geller M. J., 1990, ApJS, 74, 1

Zenteno A., et al., 2020, arXiv e-prints, p. arXiv:2004.01721

Zitrin A., Bartelmann M., Umetsu K., Oguri M., Broadhurst T., 2012, MNRAS, 426, 2944

de Vaucouleurs G., de Vaucouleurs A., Corwin Jr. H. G., Buta R. J., Paturel G., Fouqué P., 1991, Third Reference Catalogue of Bright Galaxies. Volume I: Explanations and references. Volume II: Data for galaxies between 0^h and 12^h. Volume III: Data for galaxies between 12^h and 24^h.

van den Bosch F. C., Weinmann S. M., Yang X., Mo H. J., Li C., Jing Y. P., 2005, MNRAS, 361, 1203

van den Bosch F. C., et al., 2007, MNRAS, 376, 841

van den Bosch F. C., Aquino D., Yang X., Mo H. J., Pasquali A., McIntosh D. H., Weinmann S. M., Kang X., 2008, MNRAS, 387, 79

This paper has been typeset from a TeX/LaTeX file prepared by the author.